A study of backward going p and π^- in ν_μ CC interactions with the NOMAD detector

NOMAD Collaboration

P. Astier [n] D. Autiero [h] A. Baldisseri [r] M. Baldo-Ceolin [m]
M. Banner [n] G. Bassompierre [a] N. Besson [r] I. Bird [h,i]
B. Blumenfeld [b] F. Bobisut [m] J. Bouchez [r] S. Boyd [t] A. Bueno [c,x]
S. Bunyatov [f] L. Camilleri [h] A. Cardini [j] P.W. Cattaneo [o]
V. Cavasinni [p] A. Cervera-Villanueva [h,v] A. Chukanov [f]
G. Collazuol [m] G. Conforto [h,u] C. Conta [o] M. Contalbrigo [m]
R. Cousins [j] D. Daniels [c] H. Degaudenzi [i] T. Del Prete [p]
A. De Santo [h] T. Dignan [c] L. Di Lella [h] E. do Couto e Silva [h]
J. Dumarchez [n] M. Ellis [t] T. Fazio [a] G.J. Feldman [c] R. Ferrari [o]
D. Ferrère [h] V. Flaminio [p] M. Fraternali [o] J.-M. Gaillard [a]
E. Gangler [h,n] A. Geiser [e,h] D. Geppert [e] D. Gibin [m]
S. Gninenko [h,ℓ] A. Godley [t] J.-J. Gomez-Cadenas [h,v] J. Gosset [r]
C. Gößling [e] M. Gouanère [a] A. Grant [h] G. Graziani [g]
A. Guglielmi [m] C. Hagner [r] J. Hernando [v] D. Hubbard [c]
P. Hurst [c] N. Hyett [k] E. Iacopini [g] C. Joseph [i] F. Juget [i]
M. Kirsanov [ℓ] O. Klimov [f] J. Kokkonen [h] A. Kovzelev [ℓ,o]
A. Krasnoperov [a,f] D. Kustov [f] V. Kuznetsov [f,h] S. Lacaprara [m]
C. Lachaud [n] B. Lakić [w] A. Lanza [o] L. La Rotonda [d]
M. Laveder [m] A. Letessier-Selvon [n] J.-M. Levy [n] L. Linssen [h]
A. Ljubičić [w] J. Long [b] A. Lupi [g] A. Marchionni [g] F. Martelli [u]
X. Méchain [r] J.-P. Mendiburu [a] J.-P. Meyer [r] M. Mezzetto [m]
S.R. Mishra [c,s] G.F. Moorhead [k] D. Naumov [f] P. Nédélec [a]
Yu. Nefedov [f] C. Nguyen-Mau [i] D. Orestano [q] F. Pastore [q]
L.S. Peak [t] E. Pennacchio [u] H. Pessard [a] R. Petti [h,o] A. Placci [h]
G. Polesello [o] D. Pollmann [e] A. Polyarush [ℓ] B. Popov [f,n]
C. Poulsen [k] J. Rico [x] P. Riemann [e] C. Roda [h,p] A. Rubbia [h,x]
F. Salvatore [o] K. Schahmaneche [n] B. Schmidt [e,h] T. Schmidt [e]

M. Sevior[k] D. Sillou[a] F.J.P. Soler[h,t] G. Sozzi[i] D. Steele[b,i]
U. Stiegler[h] M. Stipčević[w] Th. Stolarczyk[r] M. Tareb-Reyes[i]
G.N. Taylor[k] V. Tereshchenko[f] A. Toropin[ℓ] A.-M. Touchard[n]
S.N. Tovey[h,k] M.-T. Tran[i] E. Tsesmelis[h] J. Ulrichs[t]
L. Vacavant[i] M. Valdata-Nappi[d,1] V. Valuev[f,j] F. Vannucci[n]
K.E. Varvell[t] M. Veltri[u,2] V. Vercesi[o] G. Vidal-Sitjes[h]
J.-M. Vieira[i] T. Vinogradova[j] F.V. Weber[c,h] T. Weisse[e]
F.F. Wilson[h] L.J. Winton[k] B.D. Yabsley[t] H. Zaccone[r]
K. Zuber[e] P. Zuccon[m]

[a]*LAPP, Annecy, France*
[b]*Johns Hopkins Univ., Baltimore, MD, USA*
[c]*Harvard Univ., Cambridge, MA, USA*
[d]*Univ. of Calabria and INFN, Cosenza, Italy*
[e]*Dortmund Univ., Dortmund, Germany*
[f]*JINR, Dubna, Russia*
[g]*Univ. of Florence and INFN, Florence, Italy*
[h]*CERN, Geneva, Switzerland*
[i]*University of Lausanne, Lausanne, Switzerland*
[j]*UCLA, Los Angeles, CA, USA*
[k]*University of Melbourne, Melbourne, Australia*
[ℓ]*Inst. Nucl. Research, INR Moscow, Russia*
[m]*Univ. of Padova and INFN, Padova, Italy*
[n]*LPNHE, Univ. of Paris VI and VII, Paris, France*
[o]*Univ. of Pavia and INFN, Pavia, Italy*
[p]*Univ. of Pisa and INFN, Pisa, Italy*
[q]*Roma Tre University and INFN, Rome, Italy*
[r]*DAPNIA, CEA Saclay, France*
[s]*Univ. of South Carolina, Columbia, SC, USA*
[t]*Univ. of Sydney, Sydney, Australia*
[u]*Univ. of Urbino, Urbino, and INFN Florence, Italy*
[v]*IFIC, Valencia, Spain*
[w]*Rudjer Bošković Institute, Zagreb, Croatia*
[x]*ETH Zürich, Zürich, Switzerland*

Abstract

Backward proton and π^- production has been studied in ν_μ CC interactions with carbon nuclei. Detailed analyses of the momentum distributions, of the production rates, and of the general features of events with a backward going particle, have been carried out in order to understand the mechanism producing these particles. The backward proton data have been compared with the predictions of the reinteraction and the short range correlation models.

Key words: Neutrino interactions, cumulative production, intranuclear cascade, short range correlations
PACS: 13.15.+g, 13.85.Ni

1 Introduction

It is a well established experimental fact that in the high energy interactions off nuclei there are particles emitted backwards, with respect to the beam direction, which have energies not allowed by the kinematics of collisions on a free and stationary nucleon. Backward going protons are commonly observed while, in absence of nuclear effects, their production is forbidden. High energy mesons, whose production in the backward direction is only allowed up to a given momentum, are detected also, at momenta above such a limit. Since a long time [1] this effect has been used as a powerful tool to investigate nuclear structure. The models proposed to explain the origin of these particles (also called cumulative in the literature) can be divided essentially into two categories: models based on the intranuclear cascade mechanism and models based on the cumulative effect of groups of correlated nucleons/quarks.

In the *intranuclear cascade models*, the production of particles in the kinematically forbidden region (KFR) can be seen as the result of multiple scattering and of interactions of secondary hadrons, produced in the primary ν-nucleon collision, with the other nucleons while they propagate through the nucleus [2]. The reinteraction or intranuclear cascade (INC) models usually rely on Monte Carlo methods to make their predictions [3], [4]. The importance of the intranuclear cascade mechanism is that it can provide information on the space–time evolution of the hadronization process. Experimentally one observes that the cascade is restricted to slow particles only, while the fast ones do not reinteract inside the nucleus. The currently accepted explanation for this effect is the "formation zone" concept [5]-[7]. This is the distance (or the

---

[1] Now at Univ. of Perugia and INFN, Perugia, Italy
[2] Corresponding author. *Email address:* veltri@fis.uniurb.it

time) from the production point which is required for the secondary hadrons to be "formed", i.e. to be able to interact as physical hadronic states. Since the distance/time required, due to the Lorentz time–dilation factor, is proportional to the energy of the secondary, the INC process is restricted to slow hadrons which have formation lengths smaller than the nuclear radius.

An advantage of neutrino (or more generally lepton) induced interactions with respect to hadronic processes is the fact that the projectile interacts only once, avoiding the complications related to the projectile rescattering in the target. Natural drawbacks are the facts that the equivalent of the projectile energy in the hadronic processes, i.e. the hadronic jet energy in the leptonic processes, is not fixed but varies from event to event and suffers from systematic uncertainties, especially related to the reconstruction of neutrals.

Another feature of the neutrino–nucleus interaction is the fact that, due to the extremely small neutrino–nucleon cross-section, the interaction can practically take place anywhere in the nucleus. This is not the case in hadron–nucleus (and also photon–nucleus) interactions where, due to the large cross–section, the interaction takes place essentially on the first nucleons along the particle path, i.e. on the surface of the nucleus. As a consequence not all the nucleons participate in the scattering and the total hadron–nucleus cross–section is smaller than A (the number of nucleons in the nucleus) times the total hadron–nucleon cross–section. This effect is known as *shadowing* [8].

In the *correlated nucleon/quark models* the backward particles are produced in the collisions off structures with mass larger than the mass of the nucleon. These structures are formed, at small interparticle distance, under the action of the short range part of the nuclear force. They may either be described as fluctuations of the nuclear density [9] or as clusters of a few correlated nucleons [10]-[12]. In any case these structures represent the effect of gathering two or more nucleons in small volumes with a radius of the order of $0.5 \div 0.7\ fm$. The nucleons in these structures can acquire high momenta and the fast backward going particles can be seen as a direct manifestation of the high momentum tail of the Fermi distribution. For instance, the classical mechanism of Fermi motion of nucleons inside the nucleus can explain backward proton production only up to about 300 MeV/c, well below the observed limit. Nucleons can also loose their identity in these structures and larger masses can be reached if quarks in neighbouring nucleons stick together, forming multiquark clusters [13,14]. The momentum distribution of quarks in the cluster is, in this case, responsible for the observed spectra of cumulative particles.

These two classes of models are not mutually exclusive. Indeed some features of the data can be explained by both, and the experimentally observed production in the backward hemisphere [15] can have contributions from both mechanisms.

While the production of particles in the KFR has been investigated over a very wide range of incident energies and on many different nuclear targets using hadron beams [16], the data on backward particle production in $\nu\ (\bar{\nu})$ induced reactions are far less abundant. Up to now only five bubble chamber experi-

ments have studied backward protons (and in only one experiment backward pions as well) using bubble chambers filled with deuterium [20], heavy liquid fillings [17]-[20] and in one case a hybrid emulsion–bubble chamber technique [21].

Early hadronic experiments had found that the invariant cross-section for backward particle production can be parametrized as e^{-BP^2} where P is the particle momentum. It was also found that the slope parameter B is almost independent of the type of incident particle, its energy and target type, a fact known as "nuclear scaling". Neutrino experiments have confirmed these properties.

Here we present a detailed study of backward going protons (Bp) and backward going π^- ($B\pi^-$) produced in charged current neutrino interactions in the NOMAD detector. In Sec. 2 and Sec. 3 we describe the experimental apparatus and the data treatment. In Sec. 4 we report the invariant cross section distributions of Bp and $B\pi^-$. In Sec. 5 we discuss the kinematical properties of events with a backward particle. In Sec. 6 we give the production rates and study their dependence on the atomic number using the results of other neutrino and hadron experiments as well. Finally in Sec. 7 we compare the data with the predictions of theoretical models.

2   NOMAD detector and neutrino beam

For the study of backward particles presented here, the most important component of the NOMAD detector is the active target. Its main features are highlighted here, while a detailed description of the full detector (shown in Fig. 1) can be found in Ref. [22] and [23].

The target was designed with two conflicting requirements. It had to be as light as possible in order to minimize photon conversions, multiple scattering and secondary hadronic interactions, and it had to be as heavy as possible in order to produce a large number of neutrino interactions.

This conflict was resolved using an active target (2.7 tons) of 44 drift chambers (DC), $3 \times 3m^2$ each [24], perpendicular to the beam axis. The target mass is provided by the chamber structure having an average density of 0.1 g/cm^3. The drift chamber composition is reported in Table 1, where it can be seen that carbon and elements with nearby atomic numbers represent over 90% of the total weight. For this reason we consider this study as a measurement of backward production in $\nu_\mu C$ interactions. The chambers are placed inside a 0.4 T magnetic field and provide a momentum resolution which can be parametrized as:

$$\frac{\sigma_P}{P} = \frac{0.05}{\sqrt{L}} \oplus \frac{0.008P}{\sqrt{L^5}}$$

where L is the track length in meters and P the momentum in GeV/c. The first term is the contribution from multiple scattering and the second comes from the single hit resolution.
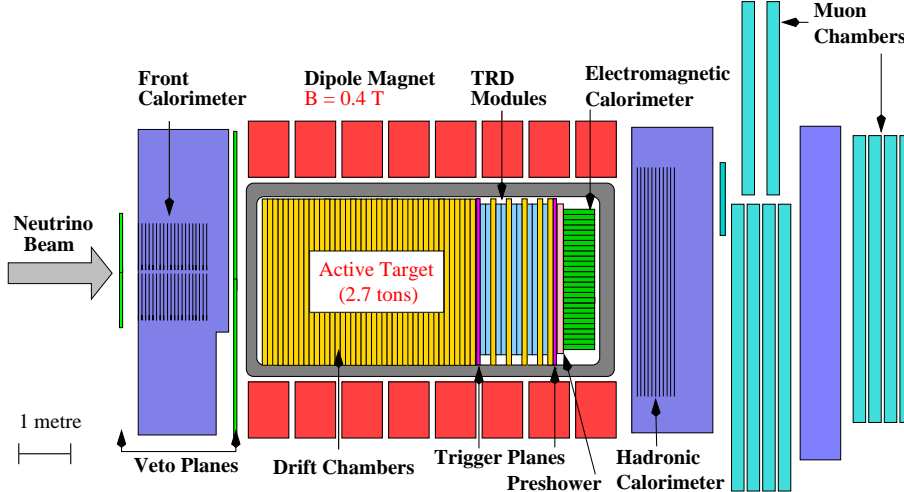

Fig. 1. *Side view of the NOMAD detector.*

Element	Z	Weight (%)	p (%)	n (%)
H/D	1	5.14	5.09	0.05
C	6	64.30	32.12	32.18
N	7	5.92	2.96	2.96
O	8	22.13	11.07	11.07
Al	13	1.71	0.82	0.89
Si	14	0.27	0.13	0.14
Cl	17	0.30	0.14	0.16
Ar	18	0.19	0.09	0.10
Cu	29	0.03	0.01	0.02
			52.43	47.56

Table 1
NOMAD drift chamber composition, showing the proportions by weight of atoms, and of protons and neutrons. As can be seen the target consists mainly of carbon and is practically isoscalar.

The target is followed by a transition radiation detector (TRD) [25], a preshower (PRS) and an electromagnetic calorimeter (ECAL) [26]. A hadron calorimeter and two muon stations are located just after the magnet coil. The neutrino interaction trigger [27] consists of a coincidence between two planes of counters located downstream of the active target, in the absence of a signal from a large area system of veto counters upstream of the NOMAD detector.

The CERN-SPS wide band neutrino beam is produced by $450\ GeV/c$ protons incident on a beryllium target. Neutrinos are produced in the decay of secondary pions and kaons in a $290\ m$ long decay tunnel at an average distance of $625\ m$ from the detector. The relative beam composition is predicted to be $\nu_\mu : \bar\nu_\mu : \nu_e : \bar\nu_e = 1.00 : 0.0612 : 0.0094 : 0.0024$ with average energies of 23.5, 19.2, 37.1 and 31.3 GeV respectively [28]. The average energy of muon neutrinos interacting in the apparatus is about 41 GeV.

Referring to Fig. 1 the coordinate system adopted for NOMAD has the X-axis into the plane of the figure, the Y-axis upwards and the Z-axis horizontal, approximately along the direction of the neutrino beam, which points upward, at an angle of 2.4° with respect to the Z-axis. Its origin is in the center of the front face of the first DC along the beam.

3   The data sample

3.1   Event selection

This study is based on the NOMAD full data sample collected between 1995 and 1998. In this analysis the event selection requires a primary vertex with at least 2 tracks inside the fiducial area defined by $|X| < 130\ cm$ and $-125 < Y < 135\ cm$. Along the Z direction a cut $Z_{VMIN} < Z < 400\ cm$ is imposed. Z_{VMIN} is 5 cm for the 1995 and 1996 data and is 35 cm for the data collected in 1997 and 1998. In the second period the first DC module was removed to install NOMAD–STAR [29] and the fiducial volume was slightly reduced.

To select a $\nu_\mu\ CC$ event a negative μ attached to the primary vertex, identified by the muon stations and having a momentum of at least 3 GeV/c, was required. Under these conditions the total $\nu_\mu\ CC$ sample consists of 944019 events.

3.2   Track selection

Only tracks attached to the primary vertex are used in the search for backward particles. The track is required to have at least 8 DC hits, the distance of the first hit from the primary vertex to be less than 15 cm, and the relative error on the reconstructed momentum to be less than 0.3. For the Bp search, since the identification method makes use of the momentum–range relation, tracks are required to range out in the DC volume. To avoid escaping tracks we require in addition the last hit of the track to be in a reduced fiducial volume defined by $|X| < 100\ cm$, $|Y| < 100\ cm$ and $Z_{MIN} < Z < 375\ cm$, where $Z_{MIN} = 30\ cm$ for the 1995 and 1996 data sets and $Z_{MIN} = 60\ cm$ for the

rest. Finally no secondary vertex must be found close to the last hit of the track.

3.3 MC sample

In order to estimate proton and pion reconstruction efficiencies and background we use a large sample of ν_μ CC Monte Carlo (MC) events. These events are generated using a modified version of LEPTO 6.1 [30] and JETSET 7.4 [31]. The target nucleon motion is simulated using the Fermi momentum distribution proposed by Bodek and Ritchie [33]. The generated events undergo a full detector simulation based on GEANT [32] and are subsequently reconstructed. MC events and tracks are selected in the same way as are experimental data yielding a final MC sample consisting of $\simeq 2.5 \times 10^6$ events. The MC data used for this analysis do not include the simulation of "nuclear effects" such as the intranuclear cascade or correlations [23]. When needed, specific correction procedures to the MC events are applied using the experimental data distributions (see Sec. 3.5).

3.4 Backward proton identification

Fig. 2 shows the experimental distributions of length vs. momentum for positive (left) and negative (right) tracks, going backward with respect to the beam direction, and satisfying our selection criteria.
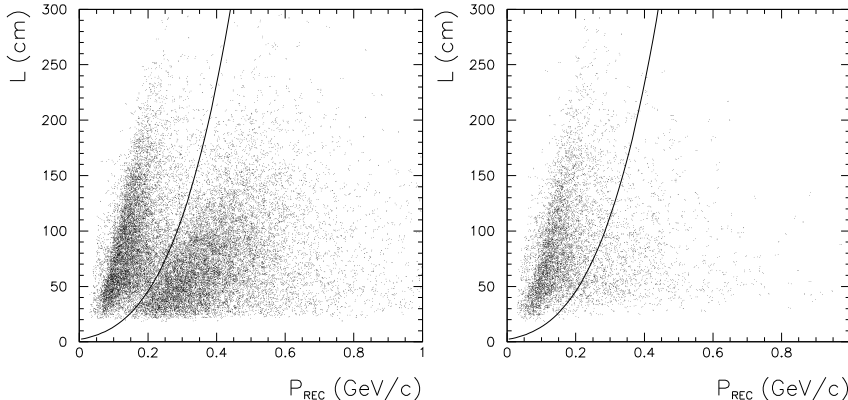

Fig. 2. *Distributions of length vs. momentum for positive (left) and negative (right) backward going tracks selected as described in the text. The line indicates the position of the cut (Eq. 1).*

Two distinct populations are clearly visible on the positive sample plot. Protons, having a shorter range than π^+, tend to accumulate in the lower right part of the plot while the π^+'s tend to populate the left–hand side. Comparing

the two plots we see that the lower right part of the negative sample is much less populated than the corresponding region of the positive one, these tracks being mainly π^-. The separation between protons and pions is also visible in Fig. 3 where the momentum distribution of positive (dots) and negative (solid line) backward tracks is shown for different intervals of track length. In this figure the heights of the negative distributions have been normalized to the positive pion peaks.

We identify as a proton any positive backward going track which passes our selection cuts and has length L:

$$L \leq 2000 \ (P_{REC} + 0.150)^{3.6} \quad cm \tag{1}$$

where P_{REC} is the reconstructed track momentum in GeV/c. The cut position was optimized by using the MC results of forward tracks and is shown in Fig. 2.
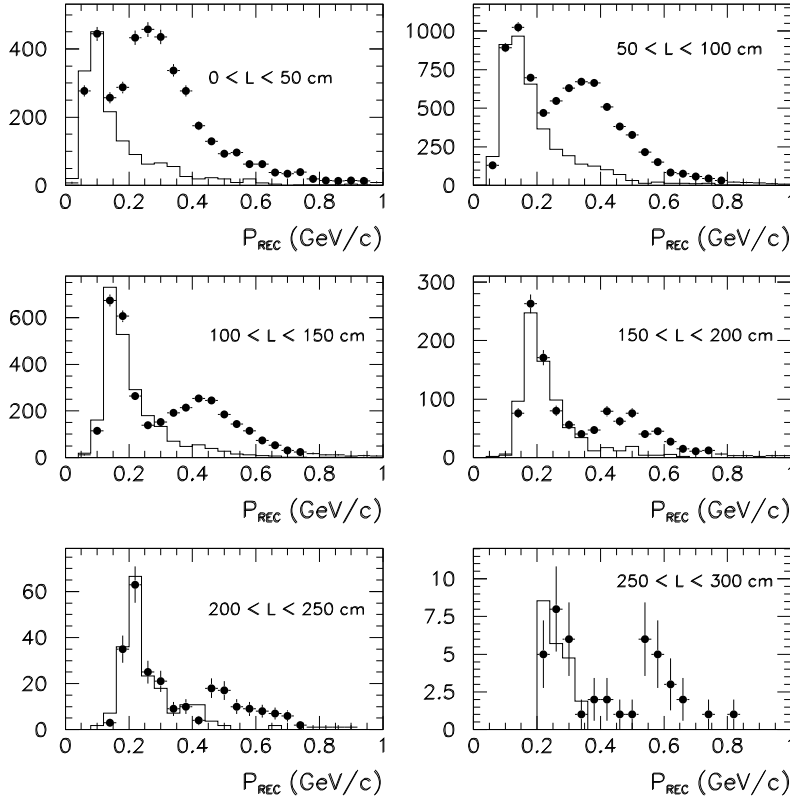
Fig. 3. *Reconstructed momentum distributions for positive (dots) and negative (solid line) backward going tracks for different intervals of the track length. The heights of the negative distributions have been normalized to the positive pion peaks.*

9

3.5 Data corrections for the Bp analysis

The reconstruction procedure used the energy loss of a pion for the track fit. Instead of refitting proton candidate tracks with the correct energy loss, an empirical correction was applied to the reconstructed proton momentum P_{REC}. This correction, which was obtained from MC events, amounts to $+180~MeV/c$ at $P_{REC} = 200~MeV/c$ and becomes negligible above $500~MeV/c$. This procedure gives the true proton momentum P.

The raw number N_p^{raw} of identified protons in a given momentum bin must be corrected for reconstruction efficiency ϵ_{REC}, stopping efficiency ϵ_{STOP}, identification efficiency ϵ_{ID} and pion contamination in the data $\pi_{cont}^{+~data}$. All these corrections will be described below. They are functions of either the reconstructed or the true proton momentum. Since the MC used for this analysis does not properly account for Bp production, some of these efficiencies can only be obtained by correcting the MC efficiencies with the data, or directly from data themselves. The "true" number N_p of protons is then:

$$N_p ~=~ N_p^{raw} ~~~ \frac{1}{\epsilon_{REC}} ~~~ \frac{1}{\epsilon_{STOP}} ~~~ \frac{1}{\epsilon_{ID}} ~~~ (1 - \pi_{cont}^{+~data}) \qquad (2)$$

with an average overall correction factor of 3.9 .

a) Reconstruction efficiency ϵ_{REC}

This is the ratio between the number of reconstructed and generated protons in a specific bin of the true momentum P and angle θ (measured with respect to the beam direction). Since this quantity depends only on the detector geometry and composition, we assume that the predictions obtained using forward going protons are applicable to the backward ones with the replacement $\cos\theta \rightarrow -\cos\theta$. An average value of 0.48 is obtained for ϵ_{REC}, the distribution of which is shown on the left in Fig. 4.

b) Stopping efficiency ϵ_{STOP}

This is the ratio between the number of backward protons fully contained in the target (Bp_{STOP}) and all the reconstructed ones (Bp). Its average value is 0.42 in the momentum range used in this analysis.

The protons are extracted from the sample of positive backward tracks by subtracting the backward π^+ content. The stopping efficiency ϵ_{STOP} is computed from the following quantities:

$$\epsilon_{STOP} = \frac{Bp_{STOP}}{Bp} = \frac{B_{STOP}^+ ~-~ B\pi_{STOP}^+}{B^+ ~-~ B\pi^+}$$

where B^+ (B_{STOP}^+) refer to backward (backward contained) positive tracks. $B\pi^+$ and $B\pi_{STOP}^+$ are the analogous quantities for backward positive pions.
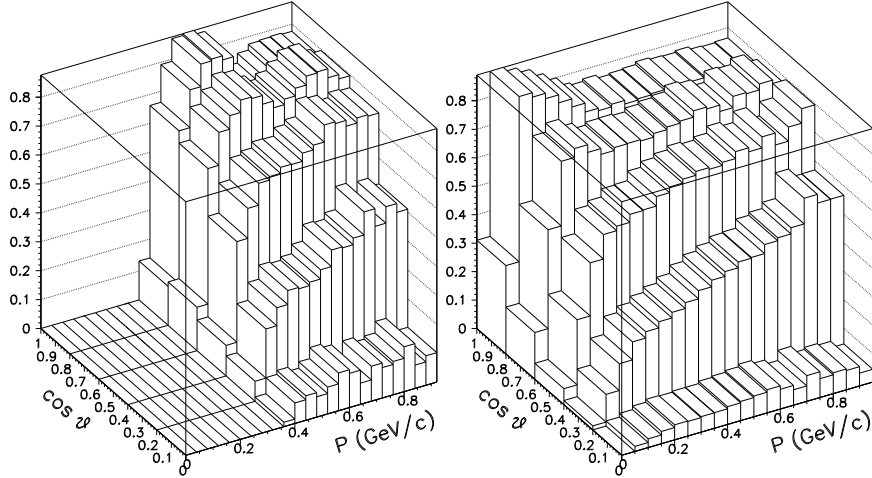
Fig. 4. *Reconstruction efficiency (as described in the text) as a function of momentum and angle between the track and the nominal beam direction. The plot on the left is for protons, the one on the right for π^-.*

They are evaluated from the data as follows.

In the NOMAD isoscalar target the length distributions of π^+ and π^-, in each momentum bin, are the same apart from a scale factor. Therefore the number of backward π^+ can be computed by the number of backward π^- once the relative population of $B\pi^+$ and $B\pi^-$ is known. The ratio of the two populations is measured from a clean sample of pions obtained by selecting tracks with a sufficiently longer length than the corresponding proton range. This ratio has comparable values for contained and not contained pions. It is almost constant in the momentum range of interest with a weighted average of $R = 1.82 \pm 0.05$.

The pion content in the backward sample is therefore:

$$B\pi^+ = R \times B\pi^- \quad ; \quad B\pi^+_{STOP} = R \times B\pi^-_{STOP}$$

where the negative pion sample ($B\pi^-$, $B\pi^-_{STOP}$) is taken to be the sample of negative (negative contained) backward tracks. This relies on the fact that the MC simulation shows that the $e^\pm$ contamination in the backward region is at the level of a few percent above $\approx 200 \; MeV/c$.

c) Identification efficiency ϵ_{ID}
This is the fraction of Bp with track length smaller than the length cut. Above $P_{REC} \simeq 300 \; MeV/c$ this quantity is 1. The results of forward going protons are applicable also in this case.

d) Pion contamination $\pi^{+\;data}_{cont}$
This is the fraction of π^+'s in the sample of identified protons, which amounts to $\approx 8\%$ above $P_{REC} \simeq 250 \; MeV/c$. To estimate this contamination in the

11

data, the MC prediction ($\pi_{cont}^{+\ MC}$) for forward particles has been corrected using the backward data distributions as follows. For each momentum bin the length distributions of protons in the data and MC can differ in normalization but not in shape since the track length depends on the mechanism of energy loss which is well reproduced by the MC. The same applies to π^{+}. The length cut applied on the momentum–length plane (Eq. 1) defines in the data and MC two populations: the π–like tracks, (the tracks above the cut) and the p–like tracks (those below the cut). To account for the difference in the populations of protons and pions in the data and MC the quantity $\pi_{cont}^{+\ MC}$ has been weighted by the double ratio of the π–like tracks (data/MC) and p–like tracks (data/MC):

$$\pi_{cont}^{+\ data} = \frac{N_{\pi^{+}}^{data}}{N_{p}^{data}} = \frac{N_{\pi-like}^{data}/N_{\pi-like}^{MC}}{N_{p-like}^{data}/N_{p-like}^{MC}} \ \pi_{cont}^{+\ MC}$$

The above correction is evaluated as a function of the reconstructed momentum.

3.6 Backward π^{-} identification

As already pointed out the e^{-} component is negligible in the negative backward track sample. We therefore assume that any negatively, backward going, charged track with $P > 0.2\ GeV/c$ is a π^{-}. The smallness of the contamination and the fact that it is not necessary to look for stopping tracks to identify the $B\pi^{-}$ reduce the number of corrections to be applied to the data to only one, the reconstruction efficiency $\epsilon_{REC}^{\pi^{-}}$.For this quantity we use the MC predictions obtained for forward going π^{-}.

The true number of negative pions is then obtained from the raw number of identified negative pions $N_{\pi^{-}}^{raw}$ in a given momentum bin according to:

$$N_{\pi^{-}} = N_{\pi^{-}}^{raw} \ \frac{1}{\epsilon_{REC}^{\pi^{-}}} \tag{3}$$

In this case the average value of the correction is 2.

4 Backward p and π^{-} invariant momentum distributions

The inclusive spectrum of backward particles is typically represented using the normalized invariant cross section $(1/\sigma_{TOT})\ E\ d^{3}\sigma/dP^{3}$, where E is the

energy of the backward going particle. The invariant cross section is usually [20] parametrized by an exponential form as:

$$\frac{1}{N_{ev}} \ \frac{E}{P} \ \frac{dN}{dP^2} \ = \ C \ e^{-BP^2} \tag{4}$$

where N_{ev} is the total number of events, C is a constant and B is the slope parameter. In previous experiments B has been found to be almost independent of the projectile type and momentum, and of the atomic number of the target. This behaviour has been termed "*nuclear scaling*" [16].
The inclusive spectrum of Bp and $B\pi^-$ is shown in Fig. 5a and 5b respectively, together with the exponential fit. The values of the measured slope parameter B are reported in Table 2. The first and the second errors are statistical and systematical, respectively.
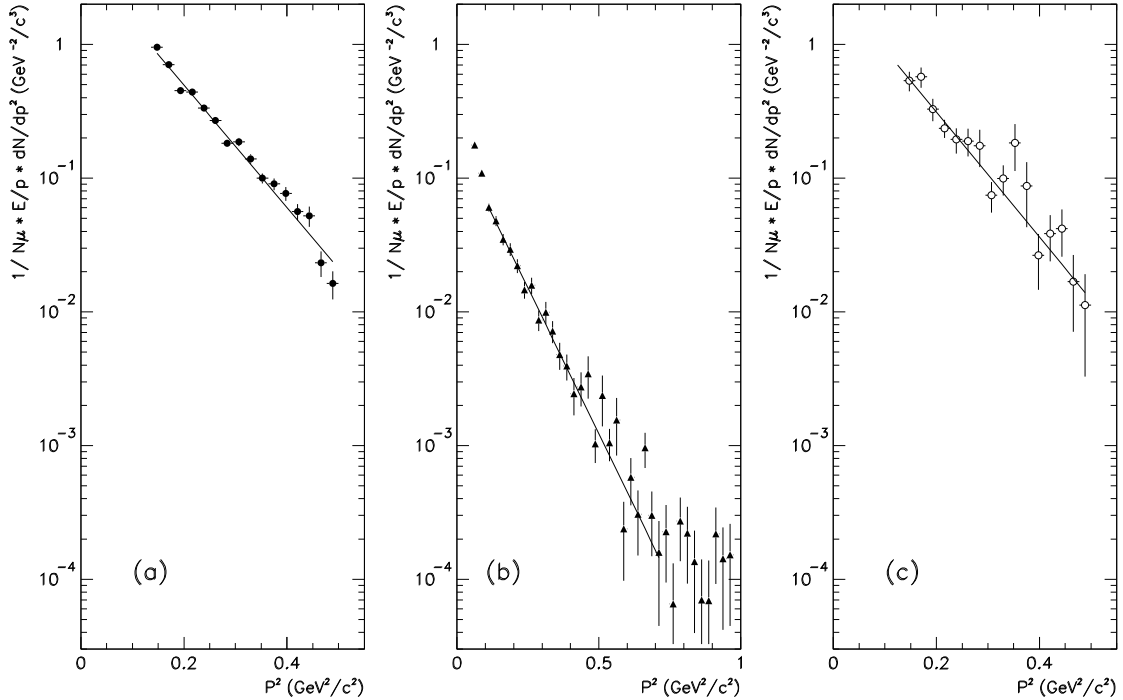
Fig. 5. *Invariant momentum distributions for backward going protons (a), π^- (b) in $\nu_\mu CC$ events and protons in $\bar{\nu}_\mu CC$ events (c)*

The systematic uncertainty was estimated by slightly changing the values of all the cuts used, by varying by a small amount the correction functions and also by changing the size of the fiducial volume. The values of the slope parameters measured in this experiment are found to be compatible with the results obtained in other neutrino (see Fig. 6 for the Bp case) and hadronic

13

		$\Delta P \ (GeV/c)$	$B(c^2/GeV^2)$	$C(c^3/GeV^2)$
Backward p	$\nu_\mu \ CC$	$0.37 \div 0.70$	$10.54 \pm 0.20 \pm 0.5$	$4.08 \pm 0.19 \pm 0.5$
	$\bar{\nu}_\mu \ CC$	$0.37 \div 0.70$	10.79 ± 0.78	2.71 ± 0.54
Backward π^-	$\nu_\mu \ CC$	$0.32 \div 0.85$	$10.03 \pm 0.28 \pm 0.3$	$0.17 \pm 0.01 \pm 0.02$

Table 2
Fit ranges and values of the slope parameter B, for backward protons and π^-, as obtained from the exponential fit to the invariant cross section. The first and the second errors are statistical and systematical, respectively.

experiments. The invariant cross section for Bp is larger than the one for
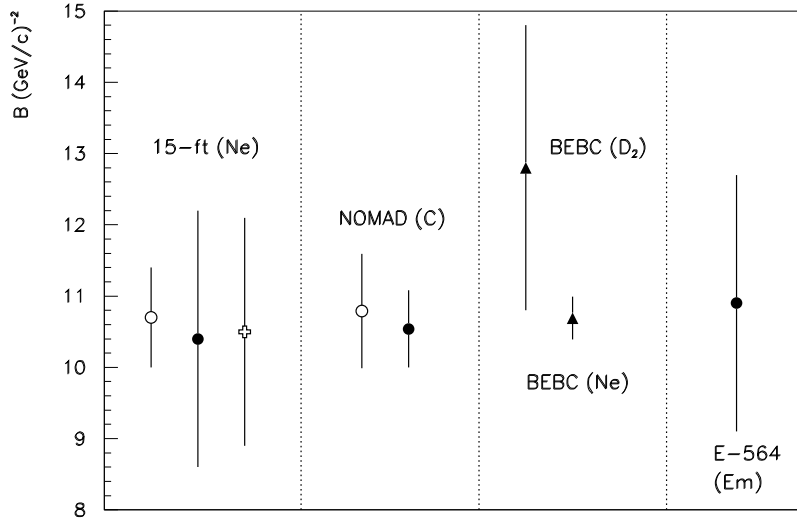
Fig. 6. *The value of the slope parameter B obtained in neutrino experiments. For NOMAD the statistical and systematical error have been added in quadrature. The full circles are the results from ν_μ CC, the open circles from $\bar{\nu}_\mu$ CC and the cross is for ν_μ NC interactions. For BEBC ν and $\bar{\nu}$ results have been combined.*

$B\pi^-$ by about one order of magnitude but the values of the slopes are similar. The kinematic ranges of the two invariant distributions are also different. To be identified Bp have to stop inside the target volume; the rather low density of the NOMAD target (see Sec. 2) restricts to $\approx 0.7 \ GeV/c$ the maximum useful momentum value.

The invariant cross section and slope parameter for Bp in $\bar{\nu}_\mu$ CC events are given in Fig. 5c and Table 2 respectively. During normal operations $\bar{\nu}_\mu$ CC events were also collected due to the small $\bar{\nu}_\mu$ component of the dominantly ν_μ beam [22]. A dedicated $\bar{\nu}$ run yielded an additional sample of $\bar{\nu}_\mu$ CC events included for this analysis.

Antineutrino events are selected under the assumptions that the efficiencies and pion contamination are the same as those used for the neutrino events, but requiring a positively charged muon instead of a negative one. The final sample consists of 61134 events containing 1764 Bp .

4.1 Energy dependence of the slope parameter

In Fig. 7 we show the slope parameter B for protons as a function of the visible hadronic energy E_{HAD} and the Q^2 of the event. The visible hadronic energy is defined as:

$$E_{HAD} = \sum E_c + \sum E_n$$

where $\sum E_c$ is the sum of the energies of reconstructed charged tracks (assuming the mass of the pion if the particle type is not explicitly identified). The sum includes all the charged tracks attached to the primary vertex by the reconstruction program, those belonging to a pointing V^0, the "close hangers" i.e. isolated tracks not associated to the primary nor to a secondary vertex and having their first hit in a box around the primary vertex of size $|X|, |Y| < 10$ cm and $-5 < Z < 20$ cm, and the "pointing hangers" i.e. the hangers which have an impact parameter of less than 10 cm when linearly extrapolated back to the z-plane of the primary vertex. $\sum E_n$ includes tracks associated to secondary vertices corresponding to interactions of neutral particles and the energy of neutral particles reconstructed in the ECAL. The reconstructed neutrino energy E_{vis} is taken to be the sum of the muon energy E_μ and of E_{HAD}. The square of the four–momentum transfer Q^2 is $Q^2 = 4\ E_{vis}E_\mu sin^2\theta/2$, where θ is the muon angle with respect to the neutrino direction. No significant dependence of the slope B on either quantity is observed, in agreement with the expectations of "nuclear scaling" as observed in hadronic beam experiments. The range covered by NOMAD is similar to the one covered by different experiments with hadronic beams.

4.2 Angular dependence of the slope parameter

The angular dependence of the slope parameter B is usually given with respect to the direction of the exchanged boson, approximated by the hadronic jet direction [20]. This allows a comparison with the results obtained in hadron beam experiments. The angular dependence of B for Bp and $B\pi^-$ is shown in Fig. 8 as a function of the angles with respect to the beam and to the hadronic jet direction. Although these two angles are highly correlated, there are small differences in the slope values. If the beam direction is used B is systematically
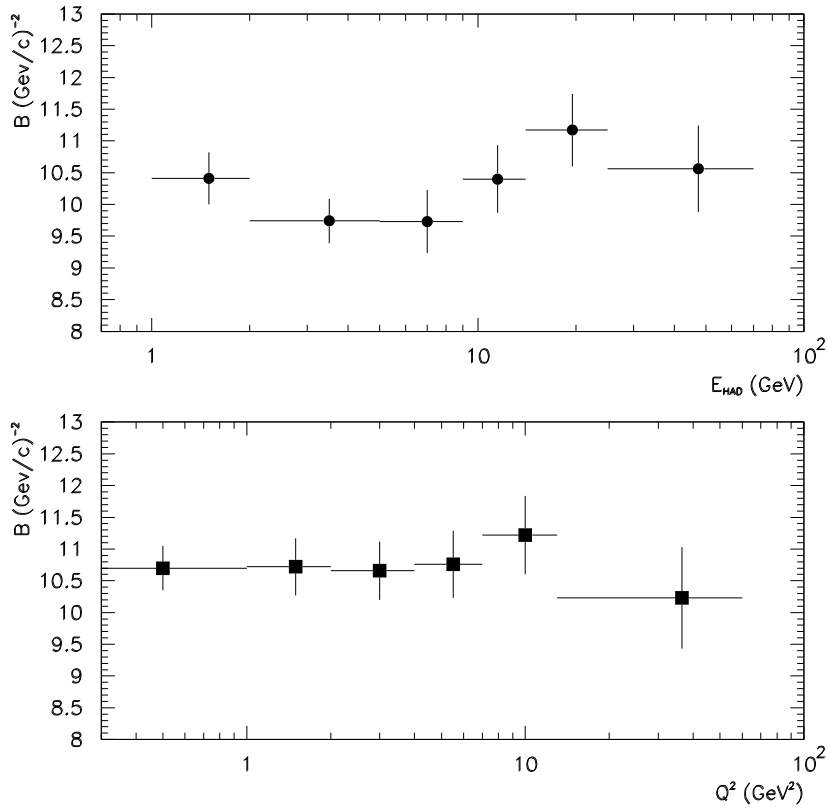
15

Fig. 7. *The value of the slope parameter B shown as a function of the hadronic energy E_{HAD} (top) and of Q^2 (bottom).*

smaller by $\approx 0.5 \div 1 (GeV/c)^{-2}$, in the Bp case, while for $B\pi^-$ the difference is less pronounced. As can be seen from Fig. 8, larger values of B are preferred at increasingly backward directions. This behaviour has already been observed in neutrino [20], photon [34] and hadron [35–37] nucleus experiments.

5 Kinematical properties of events with a backward particle

Table 3 shows a comparison of the average values of some kinematical quantities for ν_μ CC events with and without Bp or $B\pi^-$. $< C >$ and $< N^\pm >$ are the average event charge and charged multiplicity (μ^- included), $\nu = E_{vis} - E_\mu$, $x = Q^2/2M\nu$ is the Bjorken scaling variable and $W^2 = M^2 - Q^2 + 2M\nu$ is the square of the invariant mass of the hadronic system, M being the nucleon mass.

For events with a backward particle the average values of the charged multiplicity are consistent with the presence of extra tracks as expected in both models. The average value of the event charge in the Bp sample ($< C >=$ 2.11) is larger than in the no Bp, no $B\pi^-$ samples as measured in the data
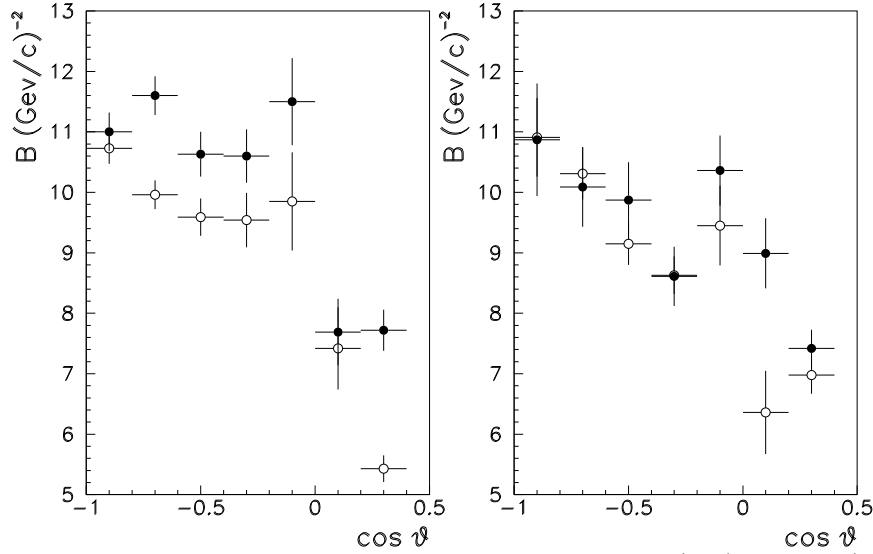
16

Fig. 8. *Angular dependence of the slope parameter B for p (left) and π⁻ (right). The value of B is shown as a function of the particle angle with respect to the hadronic jet direction (full circles) and with respect to the beam direction (open circles).*

	CC (no Bp, no $B\pi^-$)	CC (Bp)	CC ($B\pi^-$)
$< C >$	0.46	2.11±0.02	0.08±0.02
$< N^\pm >$	5.13	6.63±0.03	7.28±0.03
$< E_{vis} >$	40.75	38.9±0.4	39.5±0.5
$< E_{HAD} >$	12.32	11.4±0.2	11.7±0.2
$< Q^2 >$	7.07	5.5±0.1	5.9±0.1
$< x >$	0.32	0.26±0.002	0.28±0.003
$< W^2 >$	17.19	16.4±0.2	17.5±0.3

Table 3

Comparison of average values of some kinematical variables in events with and without an identified Bp or $B\pi^-$. The values of $< C >$ and of $< N^\pm >$ are corrected for the track reconstruction efficiency. Only statistical errors are shown. They are negligible for the first data column.

($< C >= 0.46$). It is also larger than in the total MC sample where no nuclear effects are present ($< C >= 0.31$). This observed increase is not entirely due to the bias introduced by demanding a positive particle, since an average value of $< C >= 1.21$ is obtained when requiring a backward positive track in the MC events. This can be expected from both mechanisms outlined in the Introduction. In the collisions of secondary hadrons with nucleons inside the nucleus the total event charge will increase by one unit in interactions off protons while no extra charge will be produced when scattering on neutrons. Also in the framework of the short range correlation model (in its simplest

17

form of two–nucleon correlations) the mechanism of pair breaking predicts extra tracks in the final state. The mechanism is of course symmetric for p and n but backward going neutrons are not detected.

The events with a $B\pi^-$ show an average charge smaller by $\simeq 0.4$ units with respect to the value where no $B\pi^-$ is present. Here again this effect cannot be entirely interpreted as the result of the bias associated with the requirement of at least one negative backward track, since the MC in this case predicts $< C >= -0.41$. Therefore also in the sample of events with a $B\pi^-$ an increase in the average value of the event charge is observed.

From Table 3 it appears that the average values of the kinematical variables, other than $< C >$ and $< N^{\pm} >$, for events with either a Bp or a $B\pi^-$ are systematically lower than for events without identified backward particles.

6 Backward particle rates

The Bp rate has been compared with the results of the other ν–nucleus experiments in order to study a possible atomic number dependence. In NOMAD, where Bp are identified in the momentum interval from $370 MeV/c$ to $700 MeV/c$ we obtain, after correction, the number of events reported in Table 4.

N. of Bp or $B\pi^-$	N. of Bp ev.	N. of $B\pi^-$ ev.
0	904212	939617
1	37634	4238
2	2168	164
3	5	0

Table 4
The number of events, after correction for efficiencies, as a function of the multiplicity of backward protons in the momentum interval $370 \div 700 MeV/c$, and of backward negative pions in the momentum interval $350 \div 800 MeV/c$.

These figures correspond to an average number of Bp per event, $< N_{Bp} >= (44.5 \pm 0.5) \times 10^{-3}$, where the error is statistical only. The backward proton yield obtained in other ν–nucleus experiments is shown in Table 5. The values, which were extracted from the original references, are not directly comparable because of the different momentum intervals used in the different experiments. In order to study the A dependence the Bp yields measured in NOMAD and E–564 [21] were extrapolated to the interval from 350 to 800 MeV/c assuming the dependence given in Eq. 4 with the measured slopes.
The extrapolation for NOMAD gives:

$$< N_{Bp} >_{350 \div 800 MeV/c} = \left[52.8 \pm 0.6(stat.) \pm 7(syst.) \right] \times 10^{-3}$$

Experiment	$< A >$	ΔP (GeV/c)	$< E_\nu >$ (GeV)	$< N_{Bp} >$ ($\times 10^{-3}$)	$< N_{B\pi^-} >$ ($\times 10^{-3}$)
BEBC D_2 [38]	2	0.35÷0.80	50	6.3 ± 0.7	1.0 ± 0.3
NOMAD	12	0.37÷0.70	41	44.5 ± 0.5	4.8 ± 0.1
BEBC Ne [20]	20	0.35÷0.80	50	97.7 ± 3.7	6.8 ± 0.9
15foot [17]	20	0.20÷0.80	50	137.5 ± 15	
SKAT [18]	52	0.32÷0.70	10	185.8 ± 10	
E–564 [21]	80	0.30÷0.80	60	331.1 ± 47	

Table 5
Comparison of Bp and $B\pi^-$ rates for neutrino-nucleus experiments. The average mass number $< A >$, the momentum interval ΔP used in the analysis, the average event energy $< E_\nu >$ and the Bp and $B\pi^-$ rates are listed for each experiment. The errors are purely statistical.

For E–564 we obtain $< N_{Bp} >= (234 \pm 33) \times 10^{-3}$.
The A dependence for experiments most directly comparable to NOMAD is shown in Fig. 9a. In the range $A = 20 \div 80$ it has been parametrized as $< N_{BP} > \propto A^\alpha$, where $\alpha = 0.68 \pm 0.12$ [21]. The same parametrization with a similar power law was found to describe Bp production in π^+ and K^+ collisions with Al and Au nuclei at 250 GeV/c [39]. It is evident from Fig. 9a that this simple power law does not describe the NOMAD data taken at a lower $< A >$. The $B\pi^-$ rate was directly measured in the same momentum range used for the Bp analysis. Its average value is found to be:

$$< N_{B\pi^-} >_{350 \div 800 MeV/c} = \left[4.8 \pm 0.1(stat.) \pm 0.3(syst.) \right] \times 10^{-3}$$

In this case a good fit to the two BEBC points and to the NOMAD value can be obtained using the form A^α giving $\alpha = 0.83 \pm 0.25$, as shown in Fig. 9b.

7 Comparison of data with models

7.1 E_{HAD} and Q^2 dependence of Bp and $B\pi^-$ rates

The Bp and the $B\pi^-$ rates have been studied as a function of the hadronic energy E_{HAD} and of Q^2. In both cases, shown in Fig. 10 and 11 a decrease of the yield with increasing E_{HAD} and Q^2 is observed. As pointed out in the
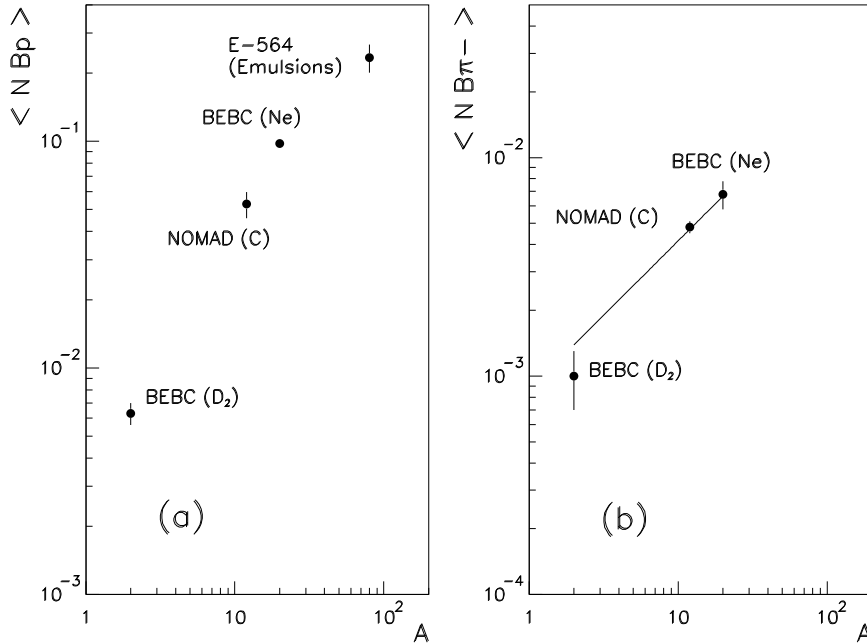
Fig. 9. *The average number of Bp per event (a) and of $B\pi^-$ per event (b) in the momentum range from $350 \div 800 MeV/c$ in neutrino experiments as a function of the mass number A. The line shown in (b) is the result of the fit described in the text.*

Introduction, this can be interpreted in terms of the "formation zone" concept. The larger E_{HAD} and Q^2, the larger is the average energy of the outgoing partons therefore resulting in hadrons which have higher probability to be formed outside the nucleus. As a consequence, reinteractions will decrease and so will the slow proton rates. This E_{HAD} and Q^2 dependence is also consistent with the decrease of the average values of E_{HAD} and Q^2 in events with identified Bp as shown in Table 3. In the $B\pi^-$ case the dependence of the yield on Q^2 and on E_{HAD} is less pronounced. This can be understood since the $B\pi^-$ rates are a less sensitive probe of nuclear effects because $B\pi^-$ production on a stationary nucleon is kinematically allowed for momenta up to about half the nucleon mass. Furthermore $B\pi^-$ can be produced in the decay of forward going resonances or unstable particles.

7.2 Multiplicities of slow particles

Since mostly slow hadrons are produced inside the nucleus, they are predominantly the ones that can scatter off nucleons, producing both slow protons and backward particles. Therefore, in the framework of the rescattering model, a correlation between the number of emitted slow protons and the multiplicity
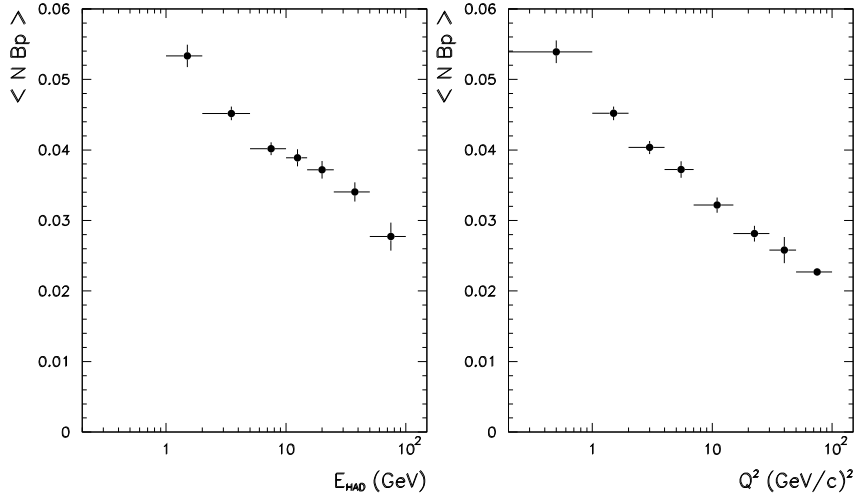
20

Fig. 10. *The average number of Bp ($370 < P < 700 MeV/c$) per event as a function of the hadronic energy E_{HAD} (left) and of Q^2 (right).*
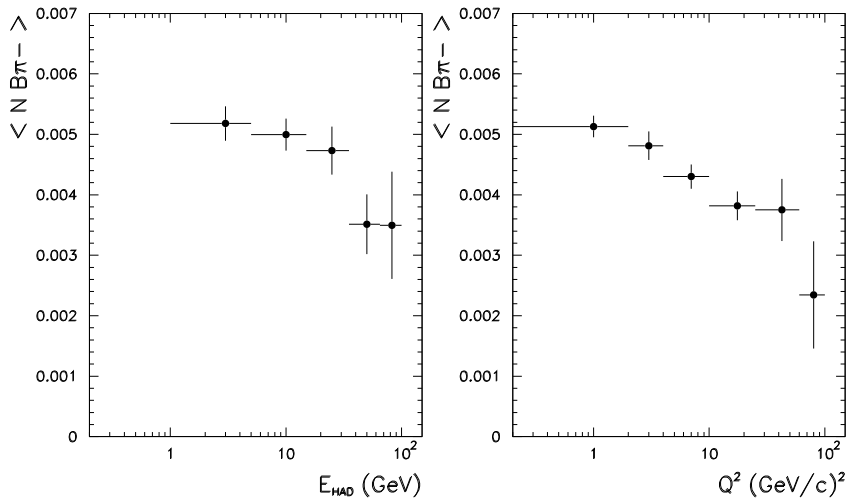

Fig. 11. *The average number of $B\pi^-$ ($350 < P < 800 MeV/c$) per event as a function of the hadronic energy E_{HAD} (left) and of Q^2 (right).*

of mesons is expected [40].

The increase in the rate of events with slow protons as a function of hadron multiplicities was first observed by the E745 collaboration [41] in a ν-Freon experiment. This correlation was used [40] to extract information on the formation zone of secondary hadrons. This effect was also observed by the BEBC collaboration[42].

We have observed this correlation by studying the fraction of events with at least one Bp as a function of the multiplicity of low momentum ($P < 700 MeV/c$) positively or negatively charged hadrons (Fig. 12). In both cases, this fraction of events increases with increasing multiplicity of low momentum tracks. However, the positive hadronic multiplicity is biased by the presence of protons from rescattering itself and therefore it is less representative of

21

the original multiplicity of positive slow hadrons from the neutrino interaction. The true correlation can therefore be better studied as a function of the multiplicity of negative slow hadrons.
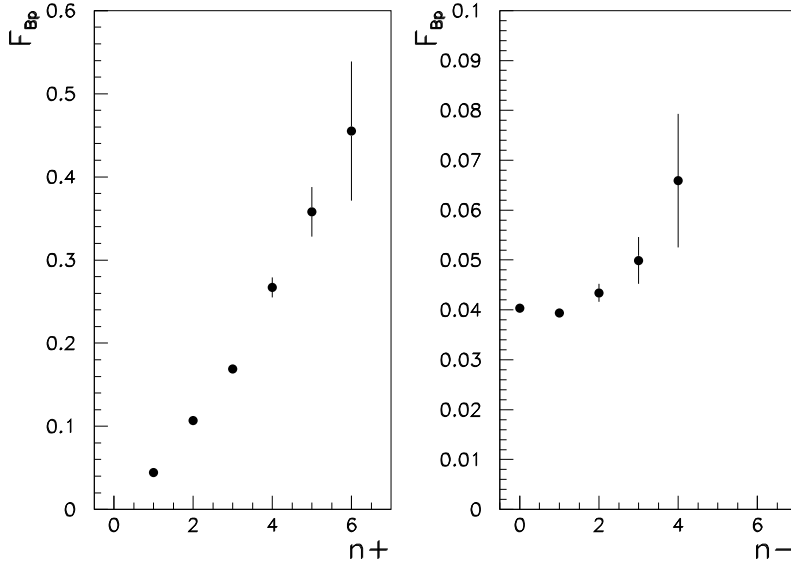

Fig. 12. *Fraction F_{Bp} of events with at least one Bp as a function of the multiplicity of low–momentum ($P < 700 MeV/c$) positively (left) or negatively (right) charged hadrons.*

7.3   Backward π^- spectra and the Fermi momentum tail

As already pointed out in the Introduction, in the short range correlation models the spectrum of fast backward going hadrons reflects the tail of the Fermi momentum distribution. For this study we used $B\pi^-$ because, as opposed to Bp, they do not need to range out in the target thus yielding data up to larger momenta.

To estimate qualitatively the contribution of this tail we have compared our $B\pi^-$ data to the predictions of two different Fermi momentum distributions [33,43]. The distribution of Ref. [33] has a long momentum tail up to 4 GeV/c. In Ref. [43] the spectrum of backward going hadrons in lepton–nucleon scattering is derived from the spectral function $p(\mathbf{k}, E)$, which is the probability of finding a nucleon with momentum $\mathbf{k}$ and removal energy E. The function, whose integral over E is the Fermi distribution, is obtained from non relativistic many body theory and a specific procedure has been developed to extrapolate it to large values of $\mathbf{k}$. In this case the Fermi momentum tail is shorter and ends at about 1 GeV/c [44].

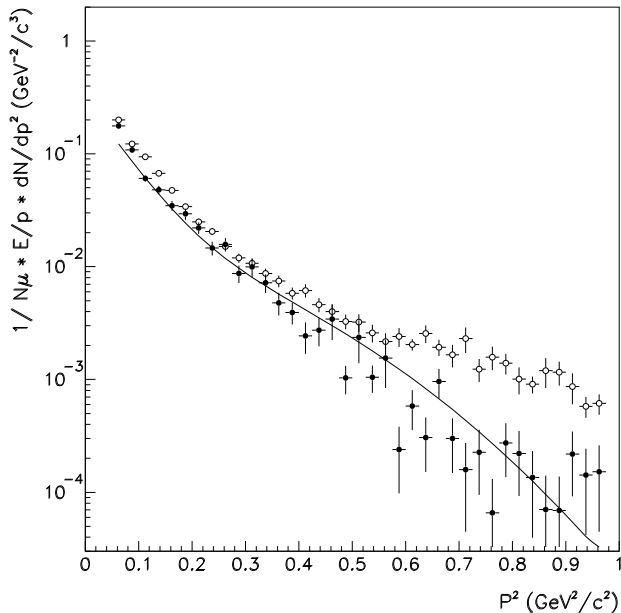In Fig. 13 the invariant spectrum of MC $B\pi^-$, simulated using the Fermi dis-

Fig. 13. *Invariant spectrum for $B\pi^-$ in MC (open circles) and data (full circles). The solid line is the curve of Ref. [43] superimposed with an arbitrary normalization.*

tribution of Ref. [33], is shown together with the data. A clear disagreement is visible in the tail of the distributions, the MC being much larger than the data above $\simeq 0.5\ (GeV/c)^2$. Our results therefore do not support a Fermi momentum distribution with a long tail as proposed in Ref. [33] while they agree with the dependence predicted by Ref. [43], as also shown in Fig. 13.

7.4 Effects of short range correlations in Bp production

According to the picture proposed in Ref. [10] Bp production is explained as the result of a neutrino interaction within a correlated cluster of two or more nucleons. This cluster is formed, for a short time, when two nucleons in their motion inside the nucleus approach each other so closely as to come under the effect of the short range component of the nuclear force ($r_c = 0.5 \div 0.7 fm$). As a result, the high relative momenta of the correlated nucleon pair manifest themselves when the backward moving spectator is released in the interaction of the incoming virtual W with the forward going nucleon. In this model, if the effects of reinteractions are neglected, the released backward nucleon can leave the nucleus keeping its original momentum. These correlated pairs have recently been observed in the reaction $e +^{16}O \ \rightarrow \ e'pp\ ^{14}C$ at low values of the energy transfer ($180 \div 240 MeV$) [45].

23

To study these correlations it is customary to use the variable α defined as:

$$\alpha = (E - P_l)/M \qquad (5)$$

where E and P_l are respectively the energy and longitudinal momentum of the Bp and M is the nucleon mass. For Bp, $\alpha > 1$ since P_l is negative. In this model, due to the target motion a correlation between the Bjorken scaling variable x and the variable α is expected. In particular the average x for events with a Bp is expected to be smaller than in events where no Bp is present, as indeed observed in our data (see Table 3). The same correlation is expected to hold if the variable $v = xy$ is used, where $y = E_{HAD}/E_{vis}$. This variable is related to the muon kinematics and can be written as :

$$v = (E_\mu - P_\mu^l)/M \qquad (6)$$

where E_μ and P_μ^l are the muon energy and longitudinal momentum. Since, generally, in neutrino experiments the muon kinematic variables are well measured, v is better suited than x for this purpose.

The (v, α) correlations were searched for in the data by calculating for each event α and v as defined in Eq. 5 and 6. For each α bin we plot the variable $< v_N >$ defined as:

$$< v_N > \quad = \quad \frac{< v >_{Bp}}{< v >_{no\ Bp}} \qquad (7)$$

where $< v >_{no\ Bp}$ is obtained from the full sample of events without a Bp. According to Ref. [10] the average values of v in events with a Bp, $< v >_{Bp}$, is related to the average value of v in events where no Bp is present, $< v >_{no\ Bp}$, by:

$$< v >_{Bp} \quad = \quad < v >_{no\ Bp} (2 - \alpha) \qquad (8)$$

More generally for a cluster composed of ξ nucleons the relation is [14]:

$$< v >_{Bp} \quad = \quad < v >_{no\ Bp} \left(1 - \frac{\alpha}{\xi}\right) \frac{\xi}{\xi - 1} \qquad (9)$$

Fig. 14a shows $< v_N >$ as a function of α. The data indicate a slope of -0.22 ± 0.06 with a $\chi^2/ndf = 5.3/6$ (the χ^2/ndf in the hypothesis of no dependence on α is 19.1/7). The two–nucleon correlation mechanism ($\xi = 2$, the most probable case when considering the overlapping probabilities of ξ nucleons in the nucleus) fails to describe our data. Either higher order structures are playing a leading role [14] or the observed low level of correlation is due to

24

the presence of reinteraction processes. In this case part of the Bp are emitted as a result of reinteractions in the nucleus and are not related to the target nucleon. The presence of intranuclear cascade processes could therefore dilute the existing correlation to the observed level. To test this hypothesis we tried
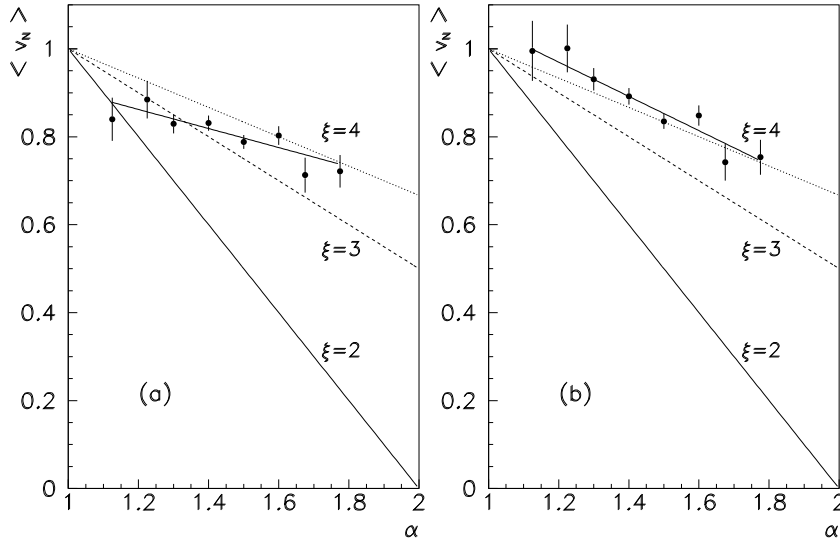

Fig. 14. *The variable $< v_N >$ plotted as a function of α. The lines represent the predicted correlation (Eq. 9) for a number ξ of nucleons in the cluster equal to 2, 3 and 4. In (a) all the Bp events were used; in (b) only events having a Bp with $cos\theta_j < 0$, θ_j being the angle of the Bp with respect to the hadronic jet direction.*

to reduce the component due to rescattering in the selected Bp sample. Having observed the correlation existing between the multiplicities of slow tracks and rescattered protons (Sec. 7.2) we applied increasingly tighter cuts on the number of slow tracks ($P < 700\ MeV/c$). As a consequence of these cuts the degree of correlation between α and v increases. The fit values of the slopes are reported in Table 6 together with the definitions of the cuts applied.

We have also observed a strong correlation between the presence of protons travelling backward in the lab but forward with respect to the hadronic jet direction, and the concentration of events at small Q^2 values and large angles with respect to the beam. Since also a small Q^2 indicates the presence of rescattering, the exclusion of these events should highlight the expected correlation. The resulting slope is -0.39 ± 0.07 with a $\chi^2/ndf = 4.9/6$ (see Fig. 14b).

The observed behaviour is consistent with the hypothesis of the correlations effects being to some degree hidden by the presence of rescattering. Reducing the rescattering component these correlations seem to become stronger.

n^+	n^-	slope	χ^2/ndf
≤ 3	≤ 2	-0.23 ± 0.06	$5.7/6$
≤ 2	≤ 1	-0.25 ± 0.07	$3.3/6$
≤ 2	0	-0.30 ± 0.07	$3.7/6$
1	0	-0.37 ± 0.10	$3.9/6$

Table 6

The fitted value of the (α, v) slope, and the corresponding χ^2/ndf, for Bp selected from events with various numbers of positive (n^+) and negative (n^-) low momentum $(P < 700 MeV/c)$ particles.

8 Conclusions

We have observed backward proton and π^- production in ν-nucleus interactions in the NOMAD detector.

The slope parameter B of the invariant cross section, parametrized as $C\,e^{-BP^2}$, has been measured and found to be consistent with previous ν-nucleus and hadron-nucleus experiments. We found that B does not depend on E_{HAD} and Q^2 over a wide range of values. This is in agreement with the "nuclear scaling" previously observed in hadronic experiments. The observed invariant spectrum is not consistent with the existence of a "long" Fermi momentum tail as the one proposed in Ref. [33] but agrees with the prediction of Ref. [43].

The Bp rate in the NOMAD target (mainly carbon) has been measured and compared with the values obtained on different nuclei. While the A dependence for neutrino scattering on heavy nuclei is consistent with that of hadron experiments, and can be parametrized as $< N_{BP} > \propto A^\alpha$ with $\alpha = 0.68$ [21], the NOMAD result does not fit this dependence. The A dependence of $B\pi^-$ has been found to be steeper than that of Bp.

The backward proton data have been compared with the predictions of reinteractions and short range models. The observed energy dependence is consistent with the "formation zone" mechanism. The correlation between the multiplicitiy of slow $(P < 700 MeV/c)$ tracks and Bp events indicates the effects of reinteractions. However when appropriate cuts are applied in order to reduce the intranuclear cascade contributions, the correlation between the Bp and the muon scaling variable v, predicted by the short range models, becomes stronger.

Acknowledgements

References

[1] A. Baldin et al., Sov. J. Nucl. Phys. **18** (1973) 41.

[2] V. B. Kopeliovich, Phys. Rep. **139** (1986) 51.

[3] J. Ranft, Zeit. Phys. **C 43** (1989) 439;
     H. J. Mörig and J. Ranft, Zeit. Phys. **C 52** (1991) 643.

[4] A. Ferrari et al., Z. Phys. **C 70** (1996) 413.

[5] L. Stodolsky, Proc. V^{th} Int. Coll. on Multiparticle Reactions, pag. 577, Oxford 1975.

[6] G. V. Davidenko and N. N. Nikolaev, Nucl. Phys **B 135** (1978) 333.

[7] A. El Naghy and S. M. Eliseev, J. Phys. G Nucl. Part. Phys. **16** (1990) 39;
     S. M. Eliseev and B. S. Yuldashev, Sov. J. Nucl. Phys. **40** (1984) 601.

[8] M. Arneodo, Phys. Rep. **240** (1994) 301.

[9] V. V. Burov et al., Phys. Lett. **B 67** (1977) 46.

[10] L. L. Frankfurt and M. Strikmann, Phys. Lett **B 69** (1977) 93;
     Phys. Rep. **76** (1981) 215.

[11] T. Fujita, Phys Rev. Lett. **39** (1977) 174.

[12] T. Fujita and J. Hüfner, Nucl. Phys **A 314** (1979) 317.

[13] C. E. Carlson, K. E. Lassila and U. P. Sukhatme, Phys. Lett. **B 263** (1991) 277
     C. E. Carlson, J. Hanlon and K. E. Lassila, hep–ph/9902281.

[14] L. A. Kondratyuk and M. Zh. Shmatikov, Z. Phys. **A 321** (1985) 301.

[15] G. D. Bosveld, A. E. L. Dieperink and A. G. Tenner, Phys. Rev. **C 49** (1994) 2379.

[16] S. Fredriksson et al, Phys. Rep. **144** (1987) 187.

[17] J. P. Berge et al., Phys. Rev. **D 18** (1978) 1367
V. I. Efremenko et al. Phys. Rev. **D 22** (1980) 2581.

[18] A. A. Ivanilov et al., JETP Lett. **30** (1979) 362.

[19] V. V. Ammosov et al., Sov. J. Nucl. Phys. **43** (1986) 759.

[20] E. Matsinos et al. Z. Phys. **C 44** (1989) 79.

[21] M. Dayon et al. Z. Phys. **C 56** (1992) 391;
R. G. Ammar et al., JETP Lett. **49** (1989) 219.

[22] J. Altegoer et al. NOMAD Coll., Nucl. Instr. and Meth. **A 404** (1998) 96.

[23] J. Altegoer et al. NOMAD Coll., Phys. Lett. **B 431** (1998) 219.

[24] M. Anfreville et al., *"The drift chambers of the NOMAD experiment"*, hep-ex/0104012, submitted for publication in Nucl. Instrum. Methods.

[25] G. Bassompierre et al., Nucl. Instr. and Meth. **A 403** (1998) 363;
G. Bassompierre et al., Nucl. Instr. and Meth. **A 411** (1998) 63.

[26] D. Autiero et al., Nucl. Instr. and Meth. **A 372** (1996) 556;
D. Autiero et al., Nucl. Instr. and Meth. **A 373** (1996) 358;
D. Autiero et al., Nucl. Instr. and Meth. **A 387** (1997) 352;
D. Autiero et al., Nucl. Instr. and Meth. **A 411** (1998) 285.

[27] J. Altegoer et al., Nucl. Instr. and Meth. **A 428** (1999) 299.

[28] G. Collazuol et al., Nucl. Instr. and Meth. **A 449** (2000) 609.

[29] G. Barichello et al., Nucl. Instr. and Meth. **A 419** (1998) 1.

[30] G. Ingelman, LEPTO 6.1, in Proc. of Physics at HERA, Edited by W. Buchmueller, G. Ingelman, DESY, Hamburg (1992) 1366.

[31] T. Sjöstrand, Computer Phys. Commun. **39** (1986) 347.

[32] GEANT, CERN Program Library Long Writeup W5013.

[33] A. Bodek and J. L. Ritchie, Phys. Rev. **D 23** (1981) 1070.

[34] K. V. Alanakyan et al., Sov. J. Nucl Phys **26** (1977) 539.

[35] Y. D. Bayukov et al., Phys Rev **C 20** (1979) 764.

[36] V. I. Komarov et al., Nucl Phys **A 326** (1979) 297.

[37] B.S. Yuldashev et al., Phys Rev **D 46** (1992) 45.

[38] D. Allasia et al., Zeit. Phys. **C 24** (1984) 119;
 A. G. Tenner, NIKHEF–H/86–7, NIKHEF Report.

[39] N. M. Agababyan et al, EHS/NA22 Coll., Z. Phys. **C 66** (1995) 385.

[40] C. Ishii, K. Saito and F. Takagi, Prog. of Theor. Phys. **86** (1991) 205.

[41] T. Kitagaki et al. E745 Coll., Phys. Lett. **B 214** (1988) 281.

[42] J. Guy et al., Phys. Lett. **B 229** (1989) 421.

[43] O. Benhar, S. Fantoni and G. Lykasov, Eur. Phys. J. **A 7** (2000) 3,415;
 O. Benhar et al., Phys. Rev. **C 55** (1997) 244.

[44] O. Benhar, private communication.

[45] R. Starink et al., Phys. Lett. **B 474** (2000) 33.